Plasma flow measurement in high- and low-field-side SOL and influence on the divertor plasma in JT-60U

N. Asakura [a,*], S. Sakurai [a], K. Itami [a], O. Naito [a], H. Takenaga [a],
S. Higashijima [a], Y. Koide [a], Y. Sakamoto [a], H. Kubo [a], G.D. Porter [b]

[a] *Naka Fusion Research Establishment, Japan Atomic Energy Research Institute, 801-1 Mukouyama, Naka-machi, Naka-gun,
Ibaraki-ken 311-0193, Japan*
[b] *Lawrence Livermore National Laboratory, P.O. Box 808, Livermore, CA 94550, USA*

Abstract

Three reciprocating Mach probes were installed at the high-field-side (HFS) baffle, low-field-side (LFS) midplane and just below the X-point in JT-60U tokamak in order to investigate the SOL flow pattern. Profiles of particle fluxes produced by parallel SOL flow and $E_r \times B$-drift flow were evaluated from Mach number, electron temperature, density and floating potential. The drift particle flux was dominant near the separatrix, while it became smaller than the parallel particle flux at the outer flux surfaces. Total particle fluxes towards HFS and LFS divertors were investigated at various plasma densities. The drift flux was comparable to the parallel flux at relatively low densities, while the parallel flux became dominant at high densities. Drift flux in the private flux region was also evaluated, and it contributed to produce in–out asymmetries in the divertor ion flux and particle recycling under attached divertor condition.
© 2003 Elsevier Science B.V. All rights reserved.

1. Introduction

The SOL plasma is generally considered to flow along the magnetic field lines from the main plasma edge to the divertor target, which is a strong plasma sink [1]. Control of the plasma flow in the SOL and divertor is considered important because of its implications for the exhaust of helium ash and impurity retention in a tokamak reactor. Poloidal variation of the SOL flow at low-field-side (LFS), plasma top and divertor, were determined recently using reciprocating Mach probes. For the ion ∇B drift direction towards the divertor, the SOL flow away from the LFS divertor (opposite to what one would expect from a simple picture of the plasma flow)

has been generally observed at LFS and plasma top (Alcator C-MOD [2], ASDEX-Upgrade [3], JT-60U [4], JET [5,6]). 'Flow reversal' of the SOL plasma was interpreted by a model of neutral ionization, which is enhanced above the divertor target [7], but it does not explain the experimental results that the subsonic SOL flow away from the divertor was observed at various locations around the main plasma edge. Mechanisms producing parallel SOL flow, resulting from the variation of plasma drift velocity in the torus due to poloidal asymmetries of the toroidal field, electric field and pressure gradients, were investigated [8–10]. At the same time, plasma drift flow in the private flux region was proposed as a candidate mechanism to produce in–out asymmetry in divertor particle flux (DIII-D [11–13]). Effects of drifts on the SOL flow pattern both in common and private flux regions should be established in order to understand the particle transport in magnetic configurations relevant to a tokamak reactor.
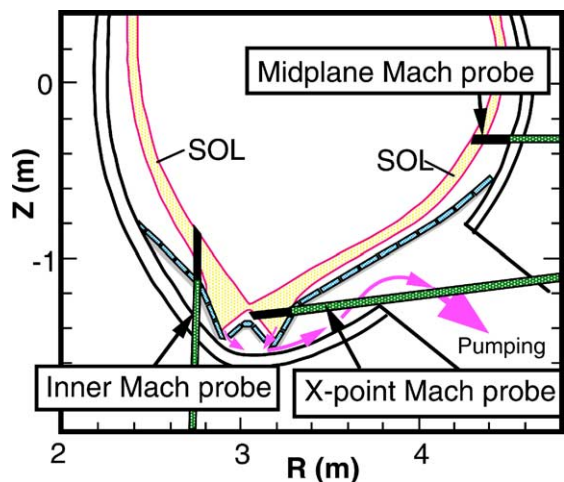

Fig. 1. Plasma cross-section and locations of reciprocating Mach probes at LFS midplane, near the X-point. New Mach probe is installed above the HFS baffle. X-point Mach probe scans from LFS divertor plate to private flux region just below the X-point. Field lines at the separatrix and $r_{mid} = 4$ cm are shown.

Determination of the SOL flow pattern and its driving mechanisms have been recently advanced in the JT-60U experiments. A reciprocating Mach probe above the inner baffle was installed, and the SOL flow profile at high-field-side (HFS) SOL was, for the first time, measured in the divertor tokamak. Measurements of the SOL flow, plasma density, temperature and potential profiles at three poloidal locations (above HFS baffle, LFS midplane and just below the X-point as shown in Fig. 1) clarified particle transport towards the HFS and LFS divertors. In this paper, the SOL flow pattern at HFS and LFS, and its dependence on the plasma density are determined in Section 2. Particle fluxes towards the HFS and LFS divertors are evaluated including parallel and perpendicular (drift) contributions. In–out asymmetry of the divertor particle flux is discussed in Section 3. Summary and conclusions are given in Section 4.

2. SOL flow and drift effects

Profiles of ion saturation currents at the upstream and downstream sides, j_s^{up} and j_s^{down}, electron temperatures, T_e^{up} and T_e^{down}, and floating potential, V_f, are measured with spatial resolution of 1–2 mm. The direction of the plasma flow along the field lines and the Mach number were deduced from the ratio of j_s^{down} to j_s^{up}, using Hutchinson's formula: $M = 0.35 \ln(j_s^{down}/j_s^{up})$ [14]. In this paper, positive and negative Mach numbers show the directions towards the LFS and HFS divertors, respectively. Parameters of the L-mode plasma are

$I_p = 1.6$ MA, $B_T = 3.3$ T, $q_{95} = 3.5$, $\delta = 0.33$, $P_{NB} = 4.3$ MW, where plasma density changes on shot-by-shot basis for normal and reversed ion ∇B drift directions. The I_p and B_t are both clockwise (CW) in the discharge (viewing from above) with the ion ∇B drift directed towards the divertor.

2.1. SOL flow pattern

Both the ion ∇B drift direction and plasma density were found to affect the plasma flow at the main plasma edge. Profiles of the Mach number measured at the three locations are shown in Fig. 2(a) and (b) for the ion ∇B drift directions towards and away from the divertor, respectively. The main plasma densities are comparable and relatively low, i.e. $\bar{n}_e = (1.6–1.7) \times 10^{19}$ m^{-3}. The profiles measured with the X-point and inner Mach probes are mapped to the LFS midplane, and the data in the private flux region are not plotted. For midplane radius (r_{mid}) of less and larger than 4 cm, field lines are connected to the divertor target and baffle, respectively.

Results of the SOL flow measurements at LFS show that flow reversal occurs at the main plasma edge for the
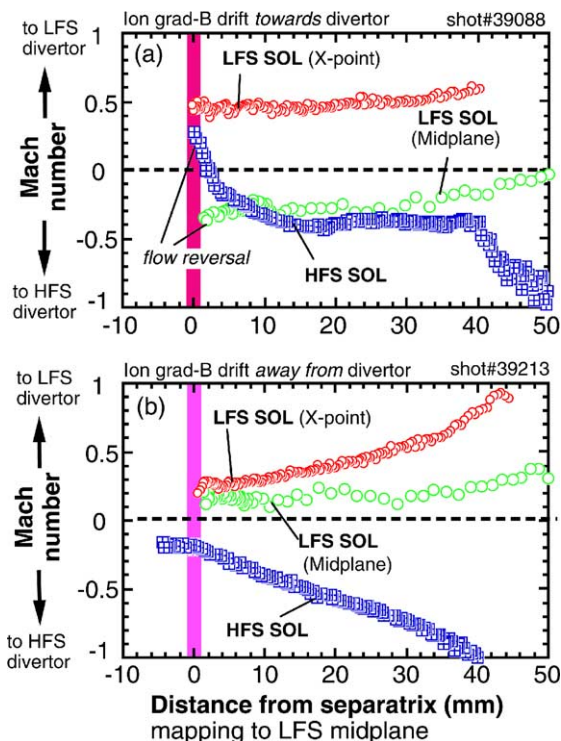

Fig. 2. Profiles of Mach number measured at three reciprocating Mach probes (at LFS midplane, near X-point and above HFS baffle) for ion ∇B drift direction, (a) towards the divertor, and (b) away from the divertor, $\bar{n}_e = (1.6–1.7) \times 10^{19}$ m^{-3}.

ion ∇B drift towards the divertor, with $M = -0.4$ near the separatrix. The flow reversal gradually reduces at outer flux surfaces, whereas fast SOL flow ($M = 0.4$) towards the LFS divertor is observed below the X-point.

The Mach number and the direction of HFS SOL flow change from the separatrix to outer flux surfaces. The SOL flow away from the HFS divertor with $M = 0.2$ is found at and outside of the separatrix, although the width of the flow reversal ($r_{mid} \sim 0.3$ cm) is narrower than that observed at LFS midplane ($\leqslant 5$ cm). Here, the flow reversal was measured in the width of 1 cm along the probe scan (Fig. 1), which was larger than the uncertainty of equilibrium calculations of ± 5 mm. Thus, the flow reversal extends outside the separatrix. On the other hand, at outer flux surfaces (1 cm $\leqslant$ $r_{mid} \leqslant 4$ cm), subsonic SOL flow towards the HFS divertor ($M \sim -0.4$) is produced. The SOL flow velocity of $|M| \sim 0.4$ is similar both at LFS midplane and HFS. Parallel SOL flow may be driven from LFS to HFS at the outer flux surfaces. We will investigate the SOL flow profiles in the two regions, i.e. near the separatrix and at outer flux surfaces. Directions of the SOL flow at three probe locations are illustrated in Fig. 3(a).

For the ion ∇B drift away from the divertor, the SOL flow towards the LFS divertor is observed both at LFS midplane and near the X-point. Mach numbers near the separatrix are similar ($M = 0.2$–0.3). The SOL flow at HFS is driven towards the HFS divertor with $M = -0.2$. These results show that the SOL flow is produced from the plasma top to the HFS and LFS divertors. Directions of the SOL flow near the separatrix for the opposite ∇B drift configurations are illustrated in Fig. 3(b). From these observations in opposite ∇B drift configurations, one concludes that the SOL flow near the separatrix of the main plasma edge, where a large influence of the plasma drift is expected, is driven against the ion ∇B drift direction.

2.2. Density dependence of SOL flow

The SOL flow velocity varies with increasing $\bar{n}_e$. Fig. 4(a) shows Mach numbers near the separatrix as a function of $\bar{n}_e/n^{GW}$, where $n^{GW} = 5.2 \times 10^{19}$ m^{-3}, for the ion ∇B drift towards the divertor. Flow reversals at LFS midplane ($|M| = 0.4$) and HFS SOL ($|M| = 0.15$) are decreased gradually with increasing $\bar{n}_e$. However, the SOL flow below the X-point increases towards the LFS divertor from $M = 0.4$ to the sonic level. This is due to the ionization front moving from the target plate to just below the X-point Mach probe as the divertor plasma detaches at the target. Finally, when the ionization front reaches near X-point during the X-point MARFE ($\bar{n}_e/n^{GW} \geqslant 0.58$), the divertor plasma downstream from the ionization front is detached and the SOL flow decreases. Ref. [4] demonstrated the divertor plasma detachment, which occurs along the field lines near the
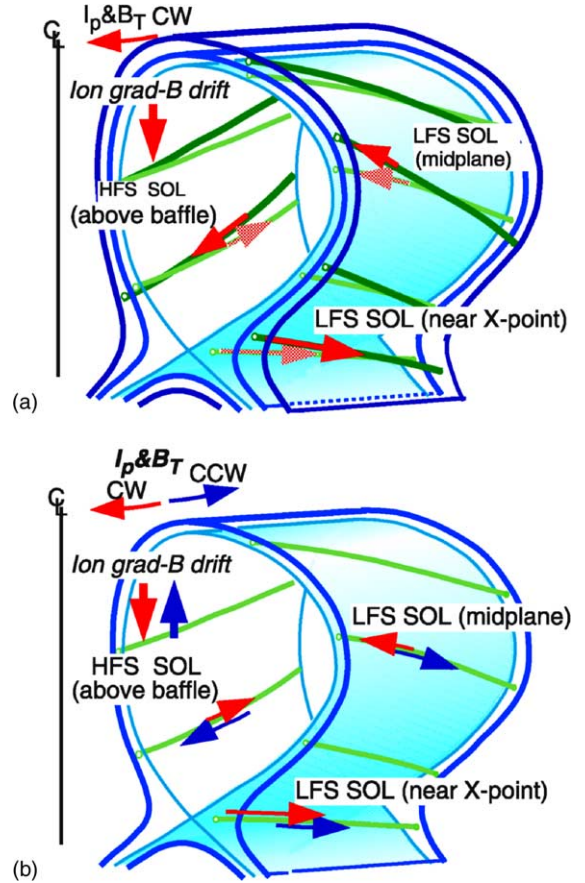

Fig. 3. Parallel SOL flow patterns (a) near the separatrix and at outer flux surfaces for the ion ∇B drift direction towards the divertor, (b) near separatrix for opposite ∇B drift configurations.

separatrix, while particle flux and the Mach number increase at outer flux surfaces.

Fig. 4(b) shows the case for the ion ∇B drift direction away from the divertor. All flow velocities at LFS midplane ($M = 0.3$), at HFS SOL ($|M| = 0.35$), and near X-point ($M = 0.35$) reduce gradually with increasing $\bar{n}_e$. The Mach number just below the X-point also becomes small (0.2) at high $\bar{n}_e$, which is different from result for the ion ∇B drift towards the divertor.

Fig. 5 shows Mach numbers at the outer flux surface ($r_{mid} = 2$ cm), for the ion ∇B drift towards the divertor. Mach numbers both above the HFS baffle and near the X-point at LFS increase with increasing $\bar{n}_e$. Here, the value of $|M| \sim 0.3$–0.5 is larger than the prediction of conventional SOL plasma model [1] ($|M| \sim 0.1$–0.2), and the mechanism which produces such a fast SOL flow is not understood yet. Particle flux density produced by the SOL flow ($n_i V_\parallel$) can be represented by $n_i M C_s \sim M j_s/e$, which also increases towards the HFS and LFS divertors. Total particle fluxes towards the divertor are
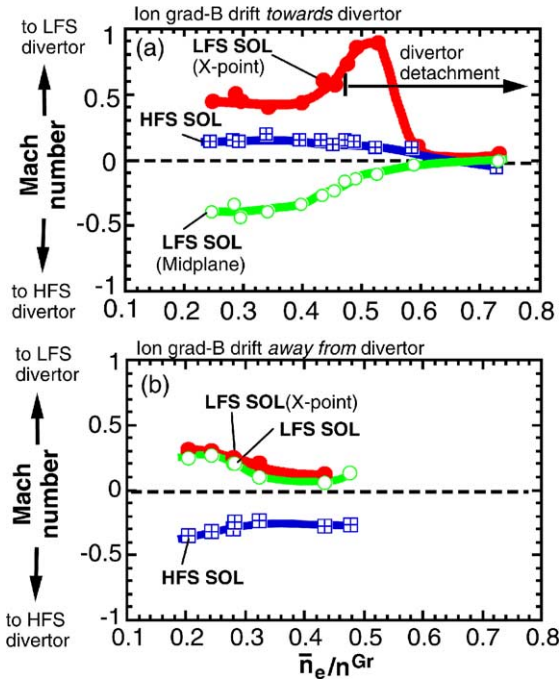
Fig. 4. Mach numbers near separatrix as a function of $\bar{n}_e/n^{Gr}$ for the ion ∇B drift (a) towards and (b) away from the divertor, $n^{Gr} = 5.2 \times 10^{19}$ m^{-3}.
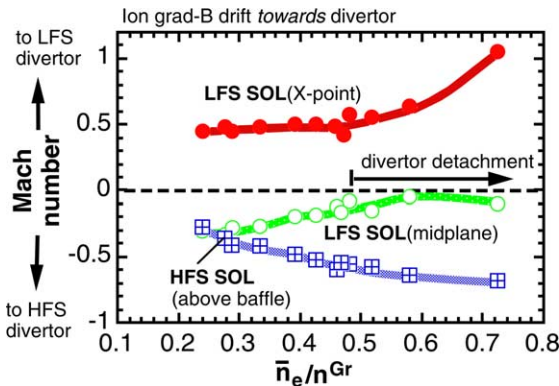

Fig. 5. Mach numbers at the outer flux surfaces ($\Delta r = 2$ cm) as a function of $\bar{n}_e/n^{Gr}$ for the ion ∇B drift direction towards the divertor.

evaluated in Section 3, including contributions of the parallel and drift flow components.

2.3. Effect of plasma drift

Poloidal drift velocity of ions is generally described by $V_{drift} = (E_r - \nabla p_i/en_i) \times B/B^2$. It is large near the separatrix due to large E_r and ∇p_i, with $E_r \times B$ drift and diamagnetic flows being in the same direction in the

SOL. At the same time, these flows vary poloidally in the torus due to variation of $B_t(= B_0[1 - (r/R)\cos\theta])$ or changes in E_r and ∇p_i. If $n_i V_{drift}$ contributes largely to the poloidal particle flux density, i.e. $V_{drift}\Phi > V_\parallel \Theta$ in $n_i V_p = n_i(V_\parallel \Theta \pm V_{drift}\Phi)$, where $\Theta = B_p/B_\parallel$ varies in torus and is much smaller than $\Phi = B_t/B_\parallel \sim 1$, the parallel plasma flow is generated to reduce asymmetry in $n_i V_{drift}\Theta$ to maintain the particle continuity and pressure balance.

According to one of candidate mechanisms to produce the flow reversal based on an asymmetry in the ion drift motion [8,15] due to the variation of B_t, the flow direction of the model is consistent with the experiments: away from the divertor at HFS and LFS SOLs for the ion ∇B drift towards the divertor and vice versa. Experimental result of a reduction in the Mach number with increasing $\bar{n}_e$ is also consistent with reduction in V_{drift} due to decreases in E_r (i.e. T_e) and T_i, and an increase in λ_{T_i} [10]. However, wide existence of the flow reversal at LFS midplane is not explained by the model only due to the variation of B_t. Two-dimensional simulation of the SOL plasma with including various $\mathbf{E} \times \mathbf{B}$, $B \times \nabla|B|$ and diamagnetic drift effects (such as UEDGE [16]) will determine their contributions to drive the parallel flow.

3. Particle fluxes towards HFS and LFS divertors

Contributions of parallel SOL flow ($n_i V_\parallel$) and drift flow ($n_i V_{drift}$) to the particle flux towards the divertor are described by their poloidal components: $n_i V_\parallel \Theta$ and $n_i V_{drift}\Phi$, respectively. The two components change with increasing $\bar{n}_e$, and the drift flow produces particle fluxes away from and towards the divertor at HFS and LFS SOLs, respectively, for the ion ∇B drift direction towards the divertor. In this section, net particle fluxes towards the HFS and LFS divertors are investigated at the Mach probe locations (above HFS baffle and near the X-point). Large $E_r \times B$ drift flow in the private flux region was pointed out in Ref. [13]. Evaluation of particle fluxes upstream of the HFS and LFS divertors and in the private flux region is crucial for determination of a mechanism producing in–out asymmetries in the divertor ion flux and particle recycling.

3.1. Particle flux produced by parallel and drift flows

Poloidal components of particle flux densities: parallel SOL flow ($n_i V_\parallel \Theta$) and $E_r \times B$ drift flow ($n_i V_{drift}^{ExB}\Phi$) are shown in Fig. 6 for the ion ∇B drift direction towards the divertor. Here, $n_i = n_e$ is assumed. Positive and negative values show the directions towards the LFS and HFS divertors, respectively. The diamagnetic flow ($n_i V_{drift}^{dia}$) is also calculated: it is comparable to $n_i V_{drift}^{ExB}$
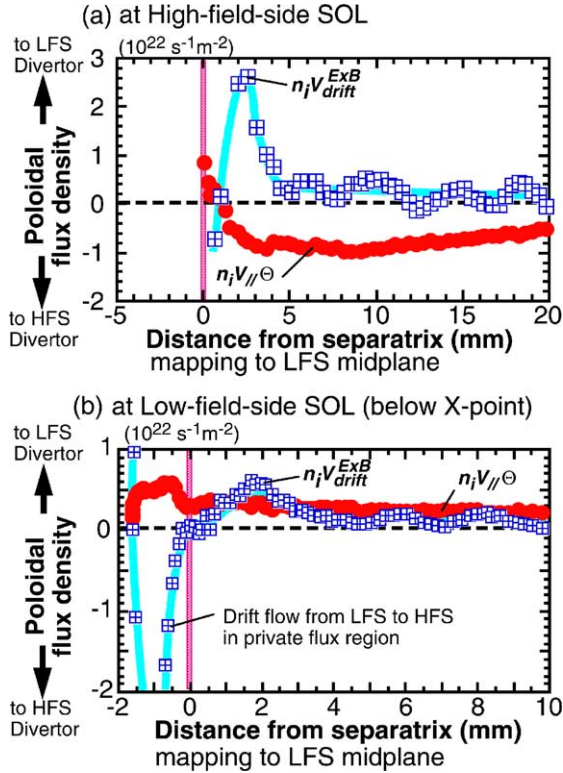
Fig. 6. Components of the poloidal flow produced by the parallel SOL flow ($n_i V_\parallel \Theta$) and $E_r \times B$ drift flow ($n_i V_{\mathrm{drift}}^{\mathrm{ExB}}$), (a) for HFS SOL, and (b) for LFS SOL, $\bar{n}_e = 1.6 \times 10^{19}$ m^{-3}. Large drift flow from LFS to HFS divertor is seen in the private flux region.
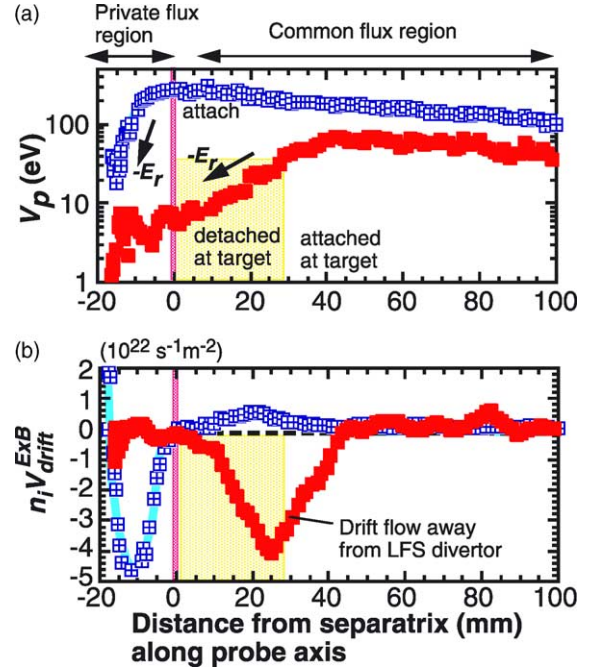

Fig. 7. Profiles of (a) plasma potential, and (b) flux density produced by $E_r \times B$ drift under attached and partially detached divertor conditions, where $\bar{n}_e = 1.6$ and 3.1×10^{19} m^{-3}, respectively.

since T_i at separatrix is a factor of 2–3 larger than T_e. However, the diamagnetic flow does not constitute the particle flux onto the divertor and it is not shown. The value of Θ changes from 0.01 (at separatrix) to 0.045 (at outer flux) near the X-point of LFS, while $\Theta = 0.05$–0.06 above HFS baffle. Near the X-point, E_r is small due to large magnetic flux expansion. Thus, $n_i V_\parallel \Theta$ and $n_i V_{\mathrm{drift}}^{\mathrm{ExB}} \Phi$ near the X-point are smaller than those near the separatrix of the main plasma. At the LFS and HFS SOLs, poloidal flux density of the drift flow is dominant near the separatrix (in 3 mm mapping to LFS midplane), and the direction is towards the LFS divertor.

Total particle fluxes towards the HFS and LFS divertors, Γ_p^{HFS} and Γ_p^{LFS}, are calculated by integrating $n_i V_\parallel \Theta$ and $n_i V_{\mathrm{drift}}^{\mathrm{ExB}} \Phi$ across the SOL along the probe scan from the separatrix to the most outer radius (r_{div}), where field line is connected to the divertor, as follows,

$$\Gamma_p^{\mathrm{HFS/LFS}} = \int_{\mathrm{sep}}^{r_{\mathrm{div}}} 2\pi R n_i [V_\parallel \Theta + V_{\mathrm{drift}}^{\mathrm{ExB}} \Phi] \nabla \psi \, \mathrm{d}r, \tag{1}$$

where positive value shows particle flux towards the LFS divertor.

Poloidal components of particle flux density in the private flux region are also shown in Fig. 6(b): $E_r \times B$ drift flux is very large and it is driven from the LFS to HFS divertor. Profiles of plasma potential (V_p) and $E_r \times B$ drift flux along the probe scan are shown in Fig. 7 for attached and partially detached divertor conditions, where V_p profile is calculated from a sheath model [1]: $V_p = 2.75 T_e + V_f$. For the attached divertor condition, $E_r \times B$ drift flow is dominant in the narrow private flux region (less than 2 cm below the X-point), and it contributes to particle transport from LFS to HFS. Fig. 7 shows changes in the detached divertor: negative E_r in the private flux region is reduced, and negative E_r appears near the boundary of detached and attached plasmas ($0 \leqslant r \leqslant 4$ cm in the common flux region). This $E_r \times B$ drift produces $n_i V_{\mathrm{drift}}^{\mathrm{ExB}}$ away from the LFS divertor to the X-point. While the large 'flow reversal' exists at the boundary of the detachment, parallel flux towards the LFS divertor in the common flux region becomes larger than the drift flux. As a result, Γ_p^{LFS} is directed towards the LFS divertor.

3.2. In–out asymmetry of divertor particle flux

First, influences of the drift flow on total particle fluxes towards the HFS and LFS divertors, Γ_p^{HFS} and Γ_p^{LFS}, are investigated. Fig. 8 shows Γ_p^{HFS}, Γ_p^{LFS} and two
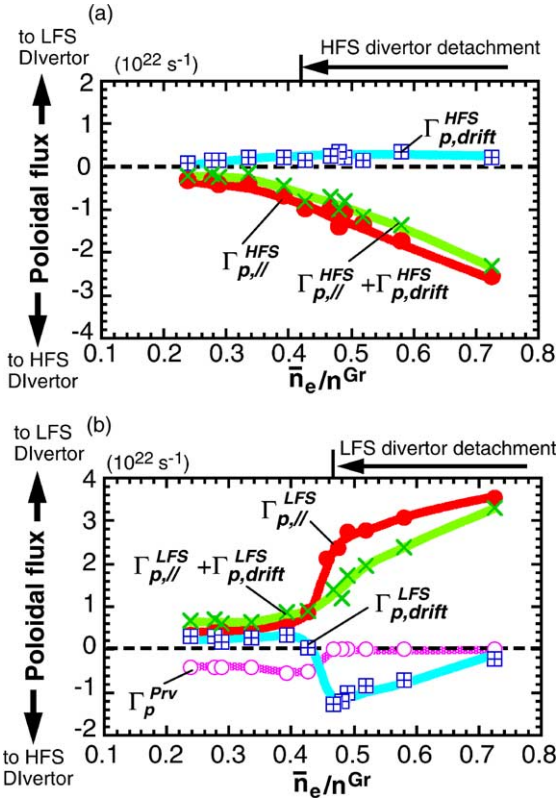
Fig. 8. Components of net poloidal flux, $\Gamma_{p,\parallel}$ and $\Gamma_{p,drift}$, produced by $n_i V_\parallel \Theta$ and ($n_i V_{drift}^{ExB}$), respectively: (a) for HFS SOL and (b) for LFS SOL. Large drift flow from LFS to HFS divertor, Γ_p^{Prv}, is seen in the private flux region under the attached divertor condition.

components corresponding to parallel flow and $E_r \times B$ drift flow as a function of $\bar{n}_e/n^{GW}$. Eq. (1) is written as $\Gamma_p^{HFS/LFS} = \Gamma_{p,\parallel}^{HFS/LFS} + \Gamma_{p,drift}^{HFS/LFS}$, where $\Gamma_{p,\parallel}^{HFS}$ and $\Gamma_{p,\parallel}^{LFS}$ are negative and positive values, respectively. $\Gamma_{p,drift}^{HFS/LFS}$ is mostly positive for the ion ∇B drift towards the divertor. Total particle flux at the private flux region, Γ_p^{Prv}, is calculated from Eq. (1), where two components measured with the X-point Mach probe are integrated in the private flux region ($-2 \leqslant r \leqslant 0$ cm).

At low $\bar{n}_e$ ($\bar{n}_e/n^{GW} = 0.24$–0.34), $|\Gamma_{p,\parallel}^{HFS}|$ of (3.0–4.0) × 10^{21} s^{-1} is a little larger than $\Gamma_{p,drift}^{HFS}$ of (0.9–2.1) × 10^{21} s^{-1}. The direction of Γ_p^{HFS} is towards the HFS divertor, and $|\Gamma_p^{HFS}|$ is (1.5–2.5) × 10^{21} s^{-1}. On the other hand, $\Gamma_{p,\parallel}^{LFS}$ and $\Gamma_{p,drift}^{LFS}$ are (3.5–4.3) × 10^{21} s^{-1} and (1.6–2.9) × 10^{21} s^{-1}, respectively. Thus, Γ_p^{LFS} is (5.9–7.0) × 10^{21} s^{-1}. As a result, Γ_p^{LFS} is larger than $|\Gamma_p^{HFS}|$, and the asymmetry is produced mostly by the drift flow near the separatrix. Here, we should consider both Γ_p^{HFS} and Γ_p^{Prv}, which are carried into the HFS divertor, in order to discuss in–out asymmetry in the divertor particle flux. $|\Gamma_p^{Prv}|$ of (3.7–3.9) × 10^{21} s^{-1} is larger than $\Gamma_{p,drift}^{LFS}$ and $\Gamma_{p,drift}^{HFS}$ as

shown in Fig. 8(b). With increasing $\bar{n}_e$, both $\Gamma_{p,\parallel}^{HFS}$ and $\Gamma_{p,\parallel}^{LFS}$ increase largely, and become dominant in particle transport towards the divertor. When the detachment occurs at LFS divertor, Γ_p^{Prv} decreases to zero and $\Gamma_{p,drift}^{LFS}$ changes the direction as described in Section 3.1.

Next, contributions of Γ_p^{HFS}, Γ_p^{LFS} and Γ_p^{Prv} to in–out asymmetry in the divertor particle flux are discussed in Fig. 9. We make the following assumptions: (i) Γ_p^{Prv} is carried into the HFS divertor, and (ii) a part of Γ_p^{LFS} is exhausted into the private flux region by diffusion and radial drifts before arriving at the target plate: such particle flux would be comparable to $|\Gamma_p^{Prv}|$. Then, total particle fluxes towards the HFS and LFS divertors are estimated as $\Gamma_p^{HFS} + \Gamma_p^{Prv}$ and $\Gamma_p^{LFS} - |\Gamma_p^{Prv}|$, respectively.

Comparison of $|\Gamma_p^{HFS} + \Gamma_p^{Prv}|$ and $\Gamma_p^{LFS} - |\Gamma_p^{Prv}|$ is shown in Fig. 9 as a function of $\bar{n}_e/n^{GW}$. For the attached divertor conditions ($\bar{n}_e/n^{GW} = 0.24$–0.45), $|\Gamma_p^{HFS} + \Gamma_p^{Prv}|$ of (5.4–12.6) × 10^{21} s^{-1} is a factor of 2–3 larger than $\Gamma_p^{LFS} - |\Gamma_p^{Prv}|$ of (2.2–4.4) × 10^{21} s^{-1}. Therefore, large contribution of Γ_p^{Prv} to the HFS-enhanced asymmetry of the divertor particle flux is determined under the attached divertor condition.

When the detachment occurs at both HFS and LFS divertors for $\bar{n}_e/n^{Gr} \geqslant 0.46$, Γ_p^{Prv} disappears and net particle fluxes towards the HFS and LFS are described as Γ_p^{HFS} ($\sim \Gamma_{p,\parallel}^{HFS}$) and Γ_p^{LFS} ($\sim \Gamma_{p,\parallel}^{LFS}$), respectively. At the same time, $\Gamma_{p,\parallel}^{LFS}$ increases larger than $\Gamma_{p,\parallel}^{HFS}$. As a result,
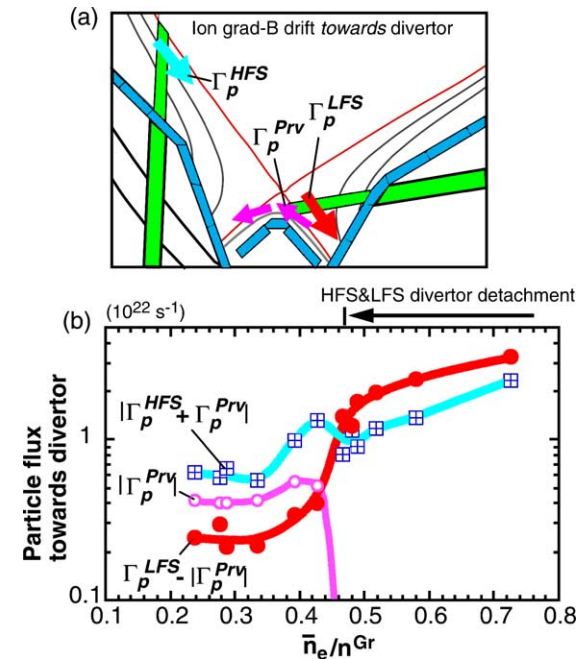

Fig. 9. (a) Directions of particle flow are illustrated at HFS, LFS and private flux region. (b) Particle fluxes towards the HFS and LFS divertors are shown as $|\Gamma_p^{HFS} + \Gamma_p^{Prv}|$ and $\Gamma_p^{HFS} - |\Gamma_p^{Prv}|$, respectively.
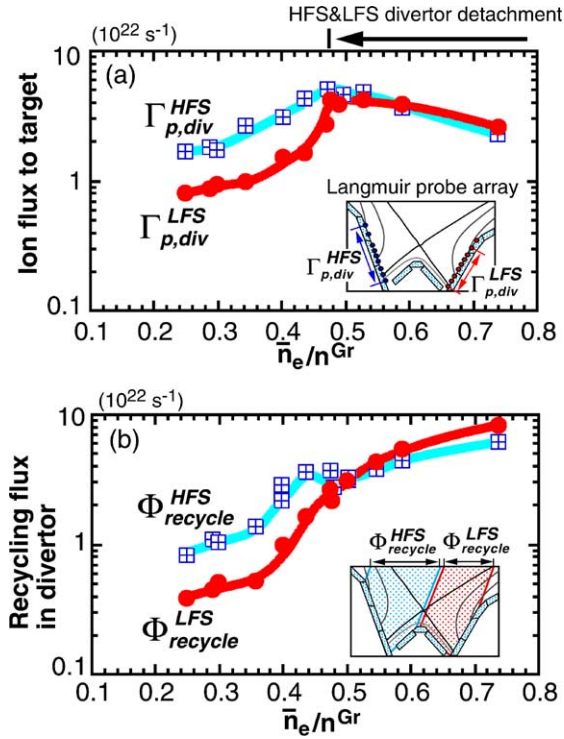
Fig. 10. (a) Total particle flux to the HFS and LFS divertor plates, and (b) total recycling fluxes in HFS and LFS divertors, as a function of $\bar{n}_e$. They are evaluated from profiles of ion saturation current and D_α brightness, respectively. Locations of target Langmuir probes and viewing area of D_α spectroscopy are also shown.

Γ_p^{LFS} becomes a factor of 1.3–1.8 larger than $|\Gamma_p^{HFS}|$. However, in–out asymmetry in Γ_p is relatively small compared to that in the attached divertor.

Similar characteristics of in–out asymmetries in the ion flux to the divertor target and the recycling flux in the divertor are generally observed. Fig. 10 shows the total ion fluxes to the HFS and LFS divertor plates, $\Gamma_{p,div}^{HFS}$ and $\Gamma_{p,div}^{LFS}$, and the total recycling fluxes in the HFS and LFS divertors, $\Phi_{recycle}^{HFS}$ and $\Phi_{recycle}^{LFS}$. They are evaluated from profiles of j_s at the target plates and D_α brightness [4]. In the attached divertor, both $\Gamma_{p,div}^{HFS}$ and $\Gamma_{p,div}^{LFS}$ are larger than $|\Gamma_p^{HFS} + \Gamma_p^{Prv}|$ and $\Gamma_p^{LFS} - |\Gamma_p^{Prv}|$, respectively. Amplification factor of the particle flux in the divertor is estimated to be relatively small (2–3). Here, ratios of $\Gamma_{p,div}^{HFS}/\Gamma_{p,div}^{LFS}$ and $\Phi_{recycle}^{HFS}/\Phi_{recycle}^{LFS}$ are 2–2.5, which are comparable to that of the net particle flux towards the divertor, $|\Gamma_p^{HFS} + \Gamma_p^{Prv}|/(\Gamma_p^{LFS} - |\Gamma_p^{Prv}|)$. When the detachment occurs at both HFS and LFS divertors, asymmetries in $\Gamma_{p,div}$ and $\Phi_{recycle}$ become small. At the highest $\bar{n}_e/n^{Gr} = 0.75$, in–out asymmetries in $\Gamma_{p,div}$ and $\Phi_{recycle}$ are reversed. These characteristics of the divertor ion flux and particle recycling are largely influenced by change in Γ_p^{HFS}, Γ_p^{LFS} and Γ_p^{Prv}.

4. Summary and conclusions

Measurements of the SOL flow both at the HFS and LFS of the JT-60U tokamak revealed the SOL flow pattern. Drift flow was dominant in a narrow region near the separatrix (corresponding to a few mm at LFS midplane), and it became smaller than the parallel SOL flow at the outer flux surfaces. Flow reversal in the parallel plasma transport was observed at both HFS and LFS near the separatrix of the main plasma, but the Mach number of this flow at HFS SOL was small and the region of this existence was narrow. The direction of the SOL flow and density dependence of the Mach number are consistent with the following model: parallel SOL flow is generated by the divergence of the drift flows in torus, to satisfy the particle continuity equation.

Evaluations of SOL particle fluxes towards the HFS and LFS divertors (Γ_p^{HFS}, Γ_p^{LFS}) and the drift flux at the private flux region (Γ_p^{Prv}) were carried out under the attached and detached divertor conditions. Influence of plasma drifts on in–out asymmetry in the divertor ion flux was large under the attached divertor condition. Γ_p^{LFS} was larger than Γ_p^{HFS}, since the drift flow is from HFS to LFS near the separatrix for the ion ∇B drift direction towards the divertor. However, large Γ_p^{Prv} significantly contributed to the HFS-enhanced asymmetry of the divertor ion flux. Under the detached divertor condition, Γ_p^{Prv} disappeared and the parallel SOL flow played an important role in the particle flux balance towards the divertor. This result explained changes of in–out asymmetries in the divertor ion flux and the recycling flux at the detachment onset.

These experimental results demonstrated the importance of the plasma drift effects for the particle transport in common and private flux regions. Code calculations with including the drift effects would be useful to optimize design of the divertor geometry and the pumping system. At the same time, application of drift effects to impurity transport would enable one to understand in–out asymmetries of helium and carbon distributions in the divertor.

References

[1] P.C. Stangeby, G.M. McCracken, Nucl. Fusion 30 (1990) 1225.

[2] B. LaBombard et al., J. Nucl. Mater. 241–243 (1997) 149.

[3] C.S. Pitcher et al., Proceedings of the 20th European Conference on Controlled Fusion and Plasma Physics, EPS, Lisboa, vol. 17C, 1993, p. 291.

[4] N. Asakura et al., Nucl. Fusion 39 (1999) 1983.

[5] A. Loarte et al., Proceedings of the 20th European Conference on Controlled Fusion and Plasma Physics, EPS, Lisboa, vol. 17C, 1993, p. 555.

[6] S.K. Erents et al., Proceedings of the 26th EPS Conference on Controlled Fusion and Plasma Physics, EPS, Maastricht, vol. 23J, 1999, p. 265.

[7] P. Cooke, A. Prinja, Nucl. Fusion 27 (1987) 1165.

[8] A.V. Chankin, P.C. Stangeby, Plasma Phys. Control. Fusion 36 (1994) 1485.

[9] A.V. Chankin, J. Nucl. Mater. 241–243 (1997) 199.

[10] N. Asakura et al., Phys. Rev. Lett. 84 (2000) 3093.

[11] T.D. Rognlien, G.D. Porter, D.D. Ryutov, J. Nucl. Mater. 266–269 (1999) 654.

[12] J.A. Boedo et al., J. Nucl. Mater. 266–269 (1999) 783.

[13] J.A. Boedo et al., Phys. Plasma 7 (2000) 1075.

[14] I.H. Hutchinson, Phys. Rev. A 37 (1988) 4358.

[15] J. Hugill, J. Nucl. Mater. 196–198 (1992) 918.

[16] G.D. Porter et al., J. Nucl. Mater., this issue. PII: S0022-3115(02)01542-8.